



# D4.5 - Report on inorganic coatings prepared by combinatorial syntheses

## VERSION

VERSION	DATE
1.0	29/01/2024

## PROJECT INFORMATION

GRANT AGREEMENT NUMBER	957189
PROJECT FULL TITLE	Battery Interface Genome - Materials Acceleration Platform
PROJECT ACRONYM	BIG-MAP
START DATE OF THE PROJECT	1/9-2020
DURATION	3 years
CALL IDENTIFIER	H2020-LC-BAT-2020-3
PROJECT WEBSITE	big-map.eu

## DELIVERABLE INFORMATION

WP NO.	4
WP LEADER	Robert Dominko
CONTRIBUTING PARTNERS	CEA, BASF, FZJ
NATURE	Report
AUTHORS	A. Benayad, F. Le Cras, M. Legallais
CONTRIBUTORS	G. Yildirim, O. Sicardy, R. Ramos, R. Fantin, W. Berthou, P. Kurzhals, I. Cekic-Laskovic
CONTRACTUAL DEADLINE	31.01.2024
DELIVERY DATE TO EC	29.01.2024
DISSEMINATION LEVEL (PU/CO)	PU

## ACKNOWLEDGMENT



This project has received funding from the European Union's Horizon 2020 research and innovation programme under grant agreement No 957189. The project is part of BATTERY 2030+, the large-scale European research initiative for inventing the sustainable batteries of the future.



## ABSTRACT

Despite its high theoretical specific capacities (>200 mAh/g), Ni-rich layered electrodes, especially  $\text{LiNi}_{0.8}\text{Mn}_{0.1}\text{Co}_{0.1}\text{O}_2$  (NMC811) and  $\text{LiNiO}_2$  (LNO) suffer from low chemical, cycling, and thermal stability. The surface engineering of these materials may overcome these critical issues. We proposed a new methodology to accelerate the discovery of artificial cathode electrolyte interphases (CEI) via a high throughput screening approach. For that, we worked with thin films, which allow direct access to the active material/electrolyte interface in 2D architecture. The idea is to deposit an artificial CEI by combinatorial synthesis above the Ni-rich layered electrode and then quickly identify which artificial CEI better protects the active material.

Consequently, task 4.5 reports the preparation of Ni-rich layered oxide thin film electrodes (NMC811 and LNO) by sputtering. The influence of the deposition parameters, the type of substrates, and the thin film crystallization are thoroughly investigated via various chemical-physical-electrochemical characterizations.

The combinatorial ionic conductor thin films synthesis in task 4.5 was de facto combined with high-throughput characterizations realized in task 6.5. Due to this strong correlation between task 4.5 and task 6.5 and to improve the readability, the synthesis and the high throughput characterizations were thoroughly reported in deliverable D6.5, which has already been submitted.

**TABLE OF CONTENTS** (if relevant)

<b>1. SYNTHESIS USING THE ALTERNATIVE MAGNETRON SPUTTERING TOOL - CEA</b> .....	<b>4</b>
1.1 ALTERNATIVE MAGNETRON SPUTTERING APPARATUS.....	4
1.2 NMC811 TARGET.....	5
1.3 INDUCTIVELY COUPLED PLASMA OPTICAL EMISSION SPECTROSCOPY CHARACTERIZATIONS.....	5
1.4 INFLUENCE OF THE SPUTTERING PARAMETERS ON THE CHEMICAL COMPOSITION OF NMC811 THIN FILMS.....	6
1.5 DEPOSITION RATE ASSESSMENT USING STYLUS PROFILOMETRY.....	7
1.6 POST-ANNEALING OF NMC811 THIN FILMS AND ITS CONSEQUENCE ON THEIR PROPERTIES.....	8
1.7 CHARACTERIZATIONS OF CRYSTALLIZED NMC811 THIN FILMS DEPOSITED ON PLATINUM DISCS.....	9
1.7.1 WORKFLOW METHODOLOGY.....	9
1.7.2 ELECTROCHEMICAL CHARACTERIZATIONS.....	10
1.7.3 STRUCTURAL ANALYSIS BY RAMAN SPECTROSCOPY.....	11
1.7.4 SURFACE ANALYSIS BY X-RAY PHOTOELECTRON SPECTROSCOPY.....	12
1.7.5 X-RAY DIFFRACTION.....	15
1.7.6 SCANNING ELECTRON MICROSCOPY.....	16
1.7.7 CONCLUSIONS.....	16
1.8 CHARACTERIZATIONS OF CRYSTALLIZED NMC811 THIN FILMS DEPOSITED ON GOLD DISCS.....	17
1.8.1 ELECTROCHEMICAL CHARACTERIZATIONS.....	17
1.8.2 CORRELATIVE ANALYSIS.....	18
<b>2. SYNTHESIS USING THE COMBINATORIAL MAGNETRON SPUTTERING TOOL AND COMPARISON – CEA/BASF</b> .....	<b>20</b>
2.1 MAGNETRON SPUTTERING APPARATUS.....	20
2.2 COMPARISON OF CHAMBER PRESSURE INFLUENCE BETWEEN SPUTTERING TOOLS.....	21
2.3 THICKNESS DISTRIBUTION OF NMC811 AND LNO THIN FILMS.....	22
2.4 CHARACTERIZATIONS OF NMC811 THIN FILMS DEPOSITED ON GOLD DISCS.....	22
2.4.1 SAMPLE PREPARATION.....	22
2.4.2 CORRELATIVE ANALYSIS.....	23
2.5 DEPOSITIONS AND CHARACTERIZATIONS OF LNO THIN FILMS, USING BASF-BASED TARGETS, ON GOLD DISCS.....	25
<b>3. HIGH-THROUGHPUT SCREENING OF THIN FILM IONIC CONDUCTOR AND LIQUID ELECTROLYTE – CEA/FZJ</b> .....	<b>27</b>
<b>4. CONCLUSIONS ABOUT THE DELIVERABLE</b> .....	<b>28</b>
<b>5. REFERENCES</b> .....	<b>29</b>



# 1. Synthesis using the alternative magnetron sputtering tool (CEA)

For the development of Ni-rich layered thin film model electrodes, the following procedure was used: firstly, obtain the proper stoichiometry within the deposited Ni-rich thin film by varying the sputtering parameters and, secondly, obtain the proper crystalline phase since the material deposited by sputtering at room temperature is amorphous. In this aim, a complete workflow combining deposition, annealing, physical-chemical characterizations and electrochemical characterizations was established to develop Ni-rich layered thin film electrode.

Note that, due to the late arrival of the ordered combinatorial sputtering tool (due to Covid-19 situation), the development of Ni-rich layered model electrodes started on alternative sputtering one. It is also integrated in a glovebox allowing the handling of as-deposited samples in Ar atmosphere. This first section reports the results obtained with this equipment.

## 1.1 Alternative magnetron sputtering apparatus

The alternative magnetron sputtering chamber is also connected to an argon glovebox, which is crucial to studying Ni-rich positive electrodes and limiting the contamination and the reactivity of the surface in contact with ambient air (details about the principle of magnetron sputtering can be found in deliverable D4.1).

We varied several parameters in order to investigate their influence on the chemical composition of the films:

- **Chamber pressure:** from 0.5 Pa to 4 Pa
- **Target power:** from 50 W to 75 W
- **Distance between the target and the substrate:** from 6 cm to 8 cm
- **Substrate locations regarding the target locations.**
- **Deposition duration:** from 3 h to 6 h

Notice that the flows of oxygen and argon ratio were fixed at 1:10.

Two different substrates were used depending on the type of characterization techniques:

- **Glass substrates** were used to study the chemical compositions by inductively coupled plasma optical emission spectroscopy (ICP-OES) and the thin film thickness by stylus profilometry. The substrates were fixed on the sample holder using Kapton tape. Centered samples are located in front of the target while eccentric is shifted compared to the normal of the target.
- **Platinum discs 12 mm in diameter and 50  $\mu\text{m}$  thick** were used to investigate the electrochemical response of the NMC thin film electrodes. Platinum was chosen for its high thermal stability under oxygen or air, as the crystallization of the ordered layered phase requires annealing temperatures as high as 700-800°C. As shown in Figure 1, a disc holder was designed to fix the platinum discs properly. This disc holder maximizes the deposition on the disc (low shading) while properly maintaining the discs.

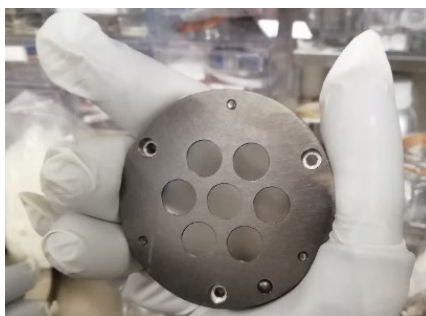


**Figure 1.** Image of the disc holder containing the platinum discs. This disc holder is then fixed on the sample holder.

## 1.2 NMC811 target

The fabrication of sputtering targets requires specific equipment, especially cold-press and mold, which were not available at UMI partners. Consequently, the  $\text{LiNi}_{0.8}\text{Mn}_{0.1}\text{Co}_{0.1}\text{O}_2$  target was purchased from another supplier (Neyco). Figure 2 depicts two images of NMC811 targets after different sputtering times. The dark spots might highlight the NMC811 grains. The spots are concentrated on an annular area. It comes from the preferential etching of the target induced by the magnetic field of the magnetron.

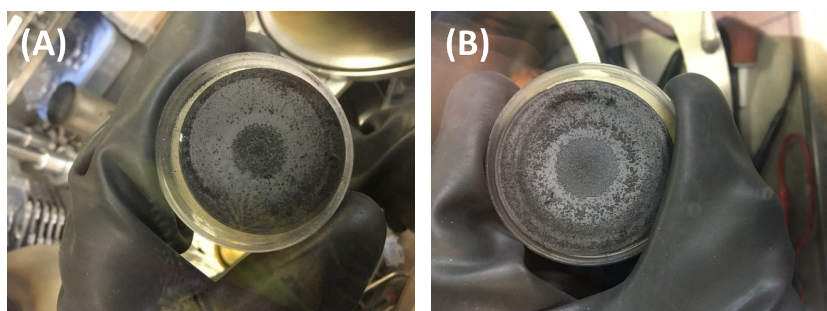


**Figure 2.** Pictures of the NMC811 target after (A) 42 h and (B) 60 h of deposition.

## 1.3 Inductively coupled plasma optical emission spectroscopy characterizations

In order to investigate the impact of the sputtering parameters on the stoichiometry of the films, the chemical compositions were systematically analyzed by ICP-OES. This technique allows the detection and quantification of all elements (Li, Ni, Mn, and Co) except O. First, thin films are dissolved in HCl solution at 3.5 % (v% in deionized water) and annealed at 60°C. Then, different solutions at different concentrations of each element were prepared using the same deionized water in order to perform calibration curves (intensity versus concentration). Note that the correlation coefficients of calibration curves were higher than 99.9. For each element, the analyzed peaks were chosen on the basis of two criteria: (i) the highest intensity (taking into account the saturation limit of the detector, especially for Li) and (ii) the lowest overlapping between neighbored peaks. Consequently, the following peaks were used:

- 610.4 nm for Li
- 238.9 nm for Co
- 257.6 nm for Mn
- 216.6 nm for Ni

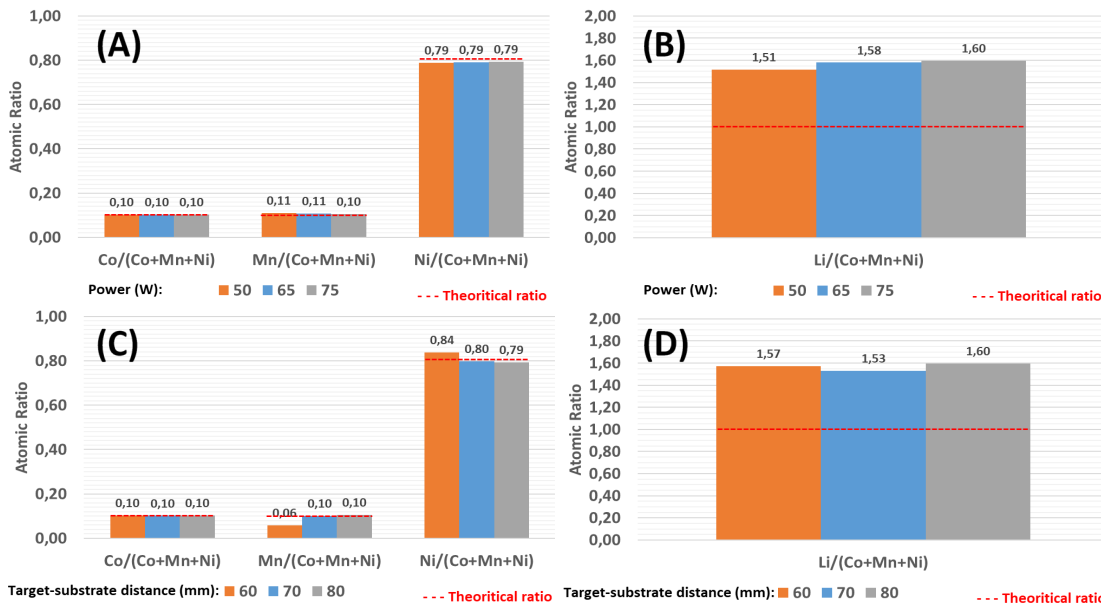


Atomic ratios presented below were calculated using the following equation.

$$\text{Atomic ratio} = \frac{C_{\text{metal}}/M_{\text{metal}}}{\sum C_{\text{metal}}/M_{\text{metal}}} \quad (\text{Equation 1})$$

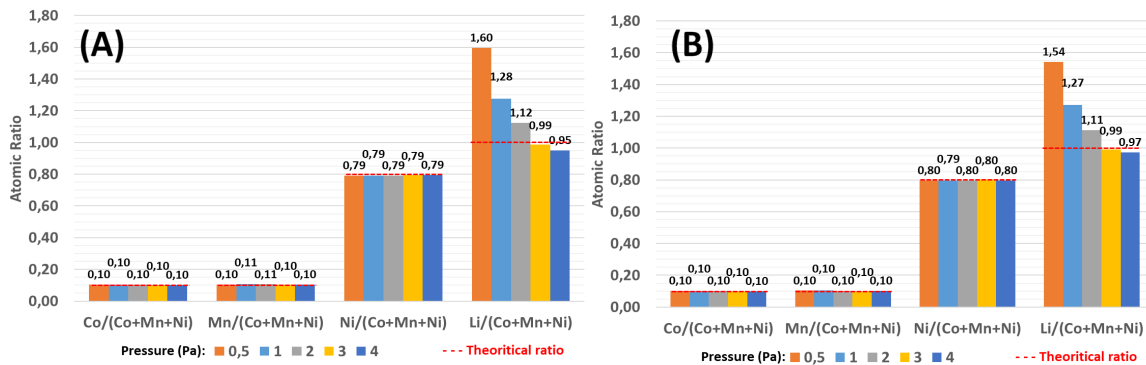
### 1.4 Influence of the sputtering parameters on the chemical composition of NMC811 thin films

Figure 3 depicts the effect of the target power and the target-to-substrate distance on the chemical composition of the NMC811 thin films prepared at a fixed pressure of 0.5 Pa. The ICP-OES results show that whatever the target power and the target-to-substrate distance, the stoichiometry of the transition metals are in agreement with expected values, while thin films are clearly Li-enriched. Both sputtering parameters have no significant impact on the chemical compositions of thin films



**Figure 3.** Impact of (A, B) the target power and (C, D) the target-to-substrate distance on the chemical compositions of the NMC811 thin films analyzed by ICP-OES. The chamber pressure was set at 0.5 Pa for both, and the deposition duration was 3 h. For (A, B), the target-to-substrate distance was fixed at 8 mm while, for (C, D), the power was set at 75 W.

We also investigated the effect of the chamber pressure and the substrate location on the stoichiometry of the films (Figure 4). Again, the chamber pressure has no relevant impact on the transition metal stoichiometry, whereas it strongly influences the Li content within the thin films. Indeed, the Li-to-transition metal ratio drops when the chamber pressure increases. At higher pressures, atoms extracted from the target may undergo more collisions within the plasma before reaching the substrate. We suggest that due to the low weight of Li atoms compared to Ar atoms in the plasma, Li will be more easily scattered than transition metals. Therefore, less Li will reach the substrate when pressure increases. Notice that the atomic ratios exhibit similar values regardless of pressure for both centered and eccentric samples. Therefore, it indicates that the chemical composition does not vary with the substrate location in this deposition area (around 5 x 5 cm<sup>2</sup>). The targeted Li<sub>1.0</sub>Ni<sub>0.80</sub>Mn<sub>0.10</sub>Co<sub>0.10</sub>O<sub>x</sub> composition is reached at a chamber pressure of 3 Pa.



**Figure 4.** Impact of (A) the chamber pressure and (B) the substrate location on the chemical compositions of the NMC811 thin films analyzed by ICP-OES. (A) and (B) represent the atomic ratio of centered and eccentric samples, respectively. For both, the target power was set at 75 W, the deposition duration was 3 h, and the target-to-substrate distance was fixed at 8 mm.

The issue related to the tuning of the Li/TM ratio in thin oxide films prepared by magnetron sputtering is often found. In the literature, the variation of the Li/TM with regard to the composition of the target is found to depend mainly on the nature of the gas and the total pressure in the chamber. When an Ar-O<sub>2</sub> mix is used, the resulting films prepared at conventional pressures are generally found to be Li-enriched [1-3]. Increasing the pressure in the deposition chamber allows the right stoichiometry to be achieved. Conversely, the trend is a Li-depleted film when pure Ar is used. In this case, preparing a Li-enriched target generally allows for a counterbalance of this effect [4-7].

To conclude, by varying several sputtering parameters (target power, target-to-substrate distance, chamber pressure, and substrate location), we identified optimal parameters to reach stoichiometry very close to the target value:

- Pressure: 3 Pa (22 mTorr)
- Oxygen: argon flow: 1:10 sccm
- RF power: 75 W
- Target-to-substrate distance: 8 cm

We also observed that the target power, the target-to-substrate distance, and the substrate location do not have a significant impact on the chemical compositions. The most relevant parameter to tune the chemical composition of the Li-Ni-Mn-Co-O thin film is the chamber pressure.

This set of conditions, which may slightly depend on some features of the sputtering device, is consistent with the appropriate conditions identified in the literature for the synthesis of related layered (Li,M)O<sub>2</sub> materials [3, 8-9].

## 1.5 Deposition rate assessment using stylus profilometry

The deposition rate was determined using profilometry. Figure 5 illustrates the deposition rate as a function of the target power for two different chamber pressure conditions. The deposition rate logically increases when the target power increases. At a higher target power, Ar ions within the plasma get higher kinetic energy; thereby, they will strongly hit the target. Consequently, the number of atoms ejected from the target per unit of time will increase, thus raising the deposition



rate. Measurements made on samples prepared at 0.5 Pa and 1.0 Pa show that the pressure does not have a noticeable influence, at least in this pressure range.

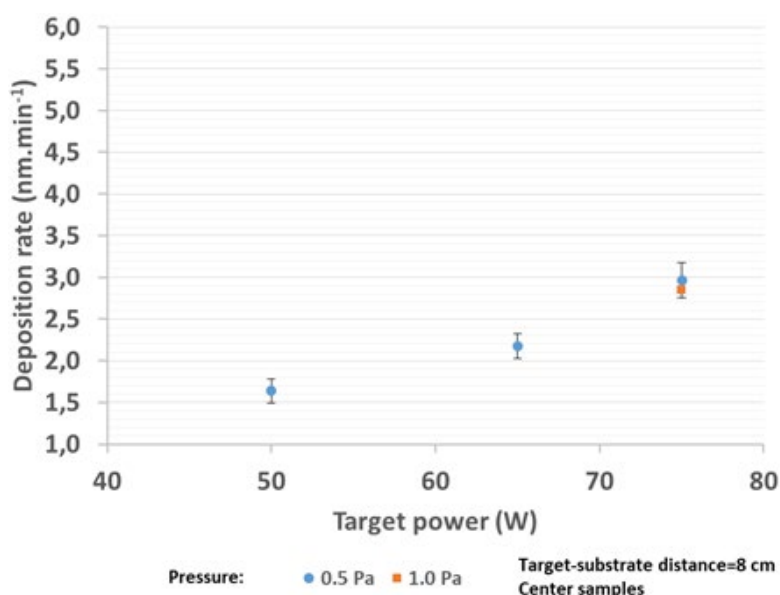


**Figure 5.** Influence of the target power on the deposition rate measured by profilometry for two different chamber pressures.

Note that the deposition rate in optimized conditions (3.0 Pa and 75 W) is about 2.4 nm.min<sup>-1</sup>.

## 1.6 Post-annealing of NMC811 thin films and its consequence on their properties

Once the suitable stoichiometry was reached in the NMC811 thin film, we investigated its crystallization. Depositions were carried out on 12 mm diameter discs cut from platinum foil for two reasons: the thermal stability of the substrate under oxidative atmosphere and its high electronic conductivity ( $\sim 10^7$  S/m) that allows introducing directly in button cells to conduct the electrochemical characterization of the thin film. Prior to film deposition, platinum discs were labelled from 1 to 7 using a diamond tip cleaned in HCl solution. Their weight was precisely determined using a microbalance (0.1  $\mu$ g resolution). Then, deposition was performed in the optimum conditions for 6 h using the disc holder shown in Figure 1. Two different runs of deposition were realized, called A and B. After deposition, samples were annealed in a tubular furnace for 10 h under oxygen flow at different temperatures (the ramp was set at 5°C/min).

**Table 1.** Condition of annealing for each sample. Annealing was carried out simultaneously for three samples (A2/A4/A6, A3/A5/A7, B2/B4/B6 and B3/B5/B6).

Sample ID	Annealing T (°C)	Sample ID	Annealing T (°C)
A2	500	B2	700
A3	600	B3	800
A4	500	B4	700
A5	600	B5	800
A6	500	B6	700
A7	600	B7	800



Annealing was carried out simultaneously for three samples (A2/A4/A6, A3/A5/A7, B2/B4/B6 and B3/B5/B6). The furnace is located outside the glovebox therefore samples were possibly exposed to ambient air for a maximum of 1 h.

After deposition, samples were weighed again in a glovebox to determine the weight of the NMC811 thin film by subtraction of the weight of the bare substrate. The result is shown in Table 2. The weight of the thin film samples varies from roughly 0.24 mg to 0.33 mg. Interestingly, from one run to another, coating weights are close regarding the sample location, indicating good reproducibility.

**Table 2.** NMC811 thin film weight after 6h of deposition in optimal conditions described earlier.

Sample ID	Coating weight (mg)	Sample ID	Coating weight (mg)
A1	-	B1	-
A2	0.263	B2	0.2777
A3	0.286	B3	0.2859
A4	0.332	B4	0.3398
A5	0.311	B5	0.3009
A6	0.279	B6	0.2926
A7	0.246	B7	0.2441

## 1.7 Characterizations of crystallized NMC811 thin films deposited on platinum discs

### 1.7.1 Workflow methodology

Prior to the high-throughput screening of bare artificial SEI/CEI film properties, we established a characterization workflow to estimate the chemical, morphological, and structural properties of reference NMC811 thin films.

The workflow is designed with respect to several strategies of acquisition trajectories, for instance:

- From non-destructive to destructive characterization methods.
- From overall coverage of a large volume of the region of interest to local view characterization. This step can be repeated at different length scales, combining two or several characterization techniques.
- Adequate sample preparation to fit with characterization techniques constraints (environment, beam size, sample holder, length and time scale acquisition, etc.).

The workflow starts by studying the chemical structure of thin films using non-destructive techniques such as X-ray photoelectron (XPS) and Raman spectroscopies. The samples were transferred from the glove box field with argon to the spectrometers through an air-tight transfer vessel.

The morphology and the crystalline structure of the films were performed using scanning electron microscopy (SEM) and X-ray diffraction (XRD) techniques.

In the meantime, similar samples were used as positive electrodes of half-coin cells and then electrochemically tested. Consequently, correlations between the electrochemical response and structural/morphological/chemical analysis of the NMC811 thin film electrodes will be realized. For clarity, the adopted workflow is illustrated in Figure 6.

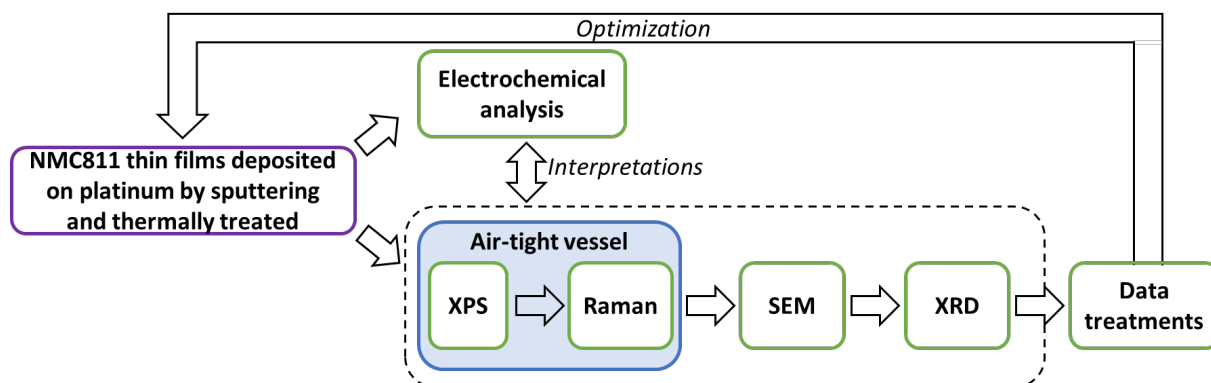


**Figure 6.** Adopted workflow methodology for the electrochemical and physical-chemical analysis of NMC811 thin films deposited by magnetron sputtering and thermally treated.

As shown in Table 1, twelve NMC811 thin films were prepared and they were characterized as follows:

- Eight samples were used as positive electrodes in half-cells (button cells) to make a first assessment of their electrochemical properties (voltage curve, specific capacity, reversibility).
- Four samples were characterized by the physical-chemical techniques using the previously described workflow.

The preliminary results are reported in the following section.

### 1.7.2 Electrochemical characterization

Electrochemical characterization was performed using a half-cell configuration in the button cell, and the annealed NMC811 thin films were deposited on platinum discs. Considering the singularity of our working electrodes in the BIG-MAP project (in particular, the absence of, or very limited, porosity), and the fact that the aim of these preliminary experiments was to identify the suitable conditions for the NMC811 thin film electrode, we used a slightly modified cell configuration compared to the BIG-MAP standard 2032 button cell. The following parts were piled up to form the 2032 button cell (Hohsen):

1. Cap
2. Gasket
3.  $\varnothing 16$  mm x 1000  $\mu\text{m}$  stainless steel spacer 1
4.  $\varnothing 16$  mm x 130  $\mu\text{m}$  Li foil
5.  $\varnothing 17$  mm Celgard 2500 separator
6. 100  $\mu\text{L}$  of LP57 electrolyte
7. NMC811 thin film deposited on  $\varnothing 12$  mm x 50  $\mu\text{m}$  Pt disc
8.  $\varnothing 16$  mm x 1000  $\mu\text{m}$  stainless steel spacer 2
9. Wave spring
10. Case

The manufacturing yield was 62.5% (5 working cells over 8).



Electrochemical analyses were performed, at 25°C, with the same procedure for all cells using a VMP3 Biologic apparatus:

1. Open circuit voltage for 5 min.
2. Five cycles at C/20 (charge and discharge) using a capacity of 200 mAh/g between 2.6 V and 4.3 V Vs Li/Li<sup>+</sup>. The current density is about 2.5-2.9 μA/cm<sup>2</sup>.
3. Open the circuit voltage for 5 minutes after each charge and discharge.

Figure 7 illustrates that the annealing temperature strongly influences the galvanostatic charge/discharge as well as the evolution of capacity. According to Figure 7(A), thin films annealed at the lowest temperature (500°C) exhibit the highest capacity with a first charge capacity as high as 170 mAh/g. Then, an increase in the annealing temperature leads to a progressive reduction of the charge/discharge capacity. Additionally, cells display important polarization in Figure 7(A) regardless of the annealing temperature. Only one plateau is visible at a potential of ~3.75 V Vs Li/Li<sup>+</sup> whereas two successive plateaus should be identifiable at 4.0 V and 4.2 V Vs Li/Li<sup>+</sup> according to literature for Ni-rich layered oxides [10], [11]. Figure 7(B) confirms that the maximum discharge capacity after each cycle decreases when the crystallization temperature increases. Two working cells based on thin films annealed at the same temperature of 500°C display reproducible discharge capacities.

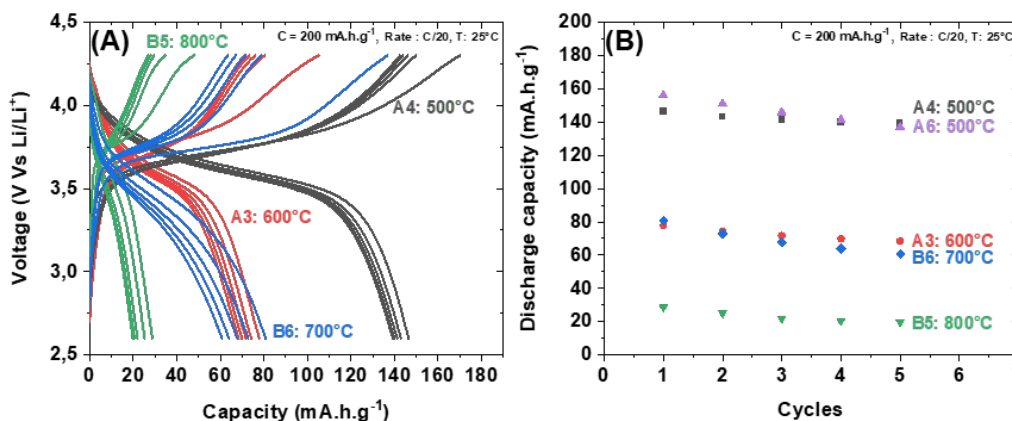


**Figure 7.** Influence of crystallization temperature on the galvanostatic charge/discharge. (A) Voltage versus capacity and (B) Discharge capacity versus cycles. Five cycles were carried out at C/20 (charge and discharge) using a 200 mAh/g capacity between 2.6 V and 4.3 V Vs Li/Li<sup>+</sup>.

### 1.7.3 Structural analysis by Raman spectroscopy

Raman analysis of thin film NMC samples was performed under a controlled environment without exposure to ambient atmosphere by directly transferring and sealing the samples inside a dedicated optical cell in an argon-filled glove box. Micro-Raman analysis in backscattering configuration (Renishaw In Via confocal microscope) was performed on multiple spots using a low-power 785 nm laser excitation to check sample uniformity. Figure 8 displays the Raman response of each sample in the spectral region of interest for NMC materials, i.e., the vibrations of the oxygen octahedron between 350 and 650 cm<sup>-1</sup>.

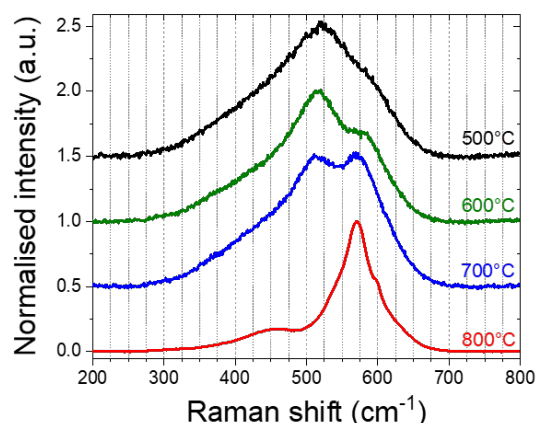


**Figure 8.** Raman spectra of thin film NMC samples annealed at various temperatures in dry air.

The four thin film samples exhibit the characteristic response of NMC811 materials in layered structure [12]. Annealing temperature modifies the relative intensities of the various bands, thus revealing a modification of the cation coordination and/or oxidation state. A thorough deconvolution of the different vibrations (i.e., six overlapping bands corresponding to bending and stretching of the oxygen octahedron around each of the three cations) would, however, be required to gain further insight into the structural modification of NMC811 thin films upon annealing. The well-defined and larger peak intensity for the sample annealed at 800°C suggests a higher crystallinity of the film.

#### 1.7.4 Surface analysis by X-ray photoelectron spectroscopy

The surface of the NMC811 thin films annealed at 500°C, 600°C, 700°C, and 800°C was investigated by XPS with a Versaprobe II spectrometer (Physical Electronics) equipped with monochromatic Al K $\alpha$  X-ray beam operated with power 50 W. The beam spot diameter was 100  $\mu\text{m}$ , and the take-off angle for photoelectron detection was 45°. All experiments were performed with both electron and Ar-ion charge neutralizations disabled under ultrahigh vacuum conditions ( $p < 10^{-7}$  Pa). High-resolution spectra were acquired with a pass energy of 29 eV, corresponding to an energy resolution of about 0.7 eV, as estimated from the FWHM of the Ag 3d $_{5/2}$  of a reference Ag sample. Peak fitting was performed using the CasaXPS software and relative sensitivity factors from the MultiPak library. The samples were transferred from the Ar-filled glovebox to the spectrometer with a dedicated transfer vessel, avoiding any contact with air. For each sample, the same measurements in three different spots were performed to verify surface homogeneity.

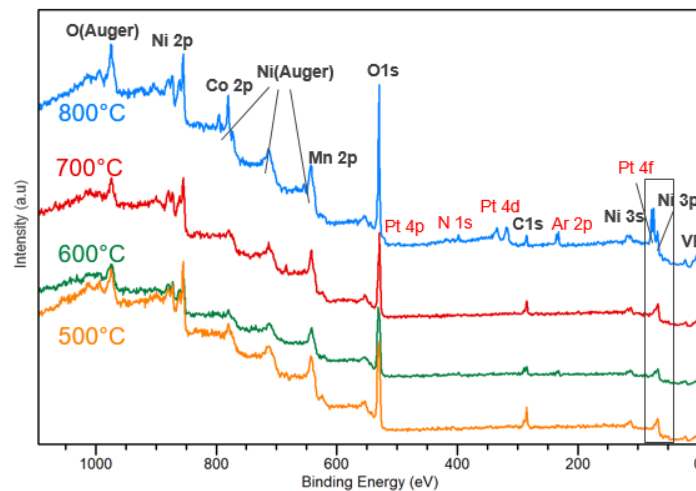


**Figure 9.** XPS survey spectra of thin film NMC811 samples annealed at various temperatures. The main Auger and core level peaks are listed.

Figure 9 shows survey spectra for the four samples. The sample annealed at 800°C exhibits additional peaks compared to the other samples, which were referred to Pt, N, and Ar contamination (red labels). Because of the nominal 8:1:1 stoichiometry, Co 2p and Mn 2p are partially covered by overlapping Ni LMM Auger peaks, which is a current issue in the analysis of Ni-rich NMC samples by most laboratory XPS's using an Al K $\alpha$  X-ray source [4].

### Surface reactivity

The peaks at about 285 eV, related to C 1s core levels, suggest the presence of carbon-based surface impurities. To study their evolution upon annealing, peak fitting analysis of C 1s high-resolution spectra was performed, as shown in Figure 10. Shirley backgrounds and Gaussian-Lorentzian GL(30) peaks were utilized for the fits. Four main components were recognized to different (semi-)organic chemical environments by comparison with reference libraries<sup>1</sup>: C-C (~284.8 eV), C-O (~285.8 eV), C=O (~288.3 eV), and O-C=O/CO<sub>3</sub><sup>2-</sup> (~289.8 eV). The latter was referred to as lithium alkylates or carbonates present on the particle surface, as confirmed by cross-analysis of O 1s and Li 1s spectra.

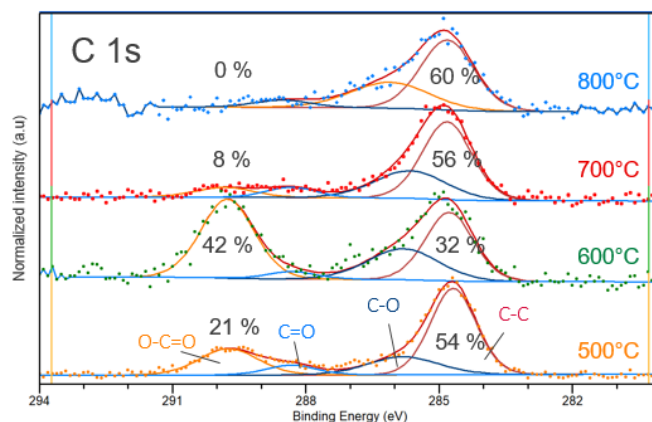


**Figure 10.** High-resolution C 1s core level spectra of thin film NMC811 samples annealed at various temperatures. Dots are experimental values, while lines are the convoluted spectra and fitted components.

<sup>1</sup> <https://srdata.nist.gov/xps/Default.aspx>



We notice an apparent decrease in lithium carbonates with increasing annealing temperature. The XPS was performed to get the oxidation states of Ni, Co, and Mn, which change with temperature and their stability.

### Qualitative and quantitative chemical composition

To get further insight into the Ni oxidation state, Ni 2p high-resolution core level spectra were qualitatively analyzed (Figure 11). The Ni 2p core level spectra are characterized by so-called “shake-up satellite” peaks between 857 and 870 eV associated with metal-ligand interaction [5]. The exact oxidation state of nickel is hard to estimate; however, the thin film of NMC shows a mixed Ni<sup>2+</sup>/Ni<sup>3+</sup> oxidation state. The ratio is still a challenge in XPS analysis and is out of the scope of this study. However, one can notice that with increasing temperature, a shoulder in the main line of Ni 2p<sub>3/2</sub> appears. This shoulder can be related to increasing Ni<sup>2+</sup> population since in pure NiO, the main line is indeed split into two peaks [15].

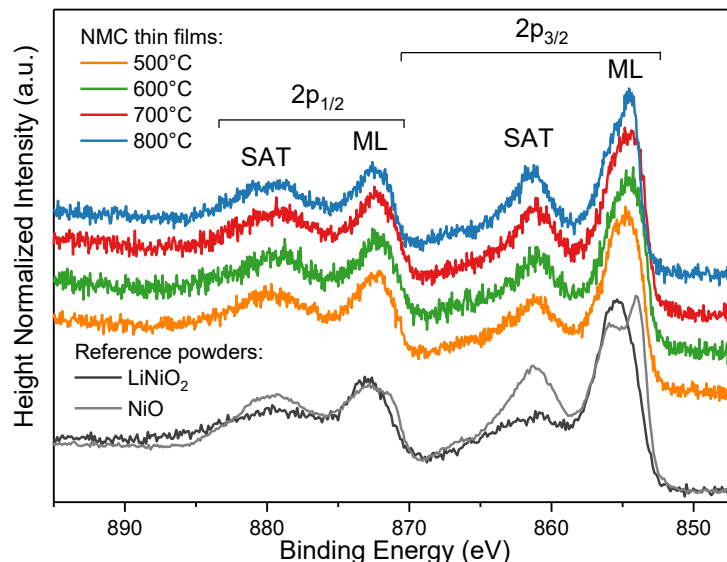


**Figure 11.** High-resolution Ni 2p core level spectra of thin film NMC811 samples annealed at various temperatures. Each spectrum was height-normalized to its maximum. Reference Ni 2p spectra of LiNiO<sub>2</sub> (BASF) and NiO (Sigma Aldrich) powders are added as a comparison. ML = main line; SAT = shake-up satellite.

High-resolution spectra were therefore recorded to semi-quantify the atomic concentration ratios of Li, Ni, Co, and Mn in NMC, shown in Figure 12. To fit the characteristic asymmetric shape of the metal 3p core levels (Ni 3p, Co 3p, and Mn 3p), an exponential blend was introduced in the GL(30) spectral shape as the first approximation. The resulting at% were then normalized to the sum of all transition metals at%. The procedure was repeated for each measurement, and the results for each sample were averaged.

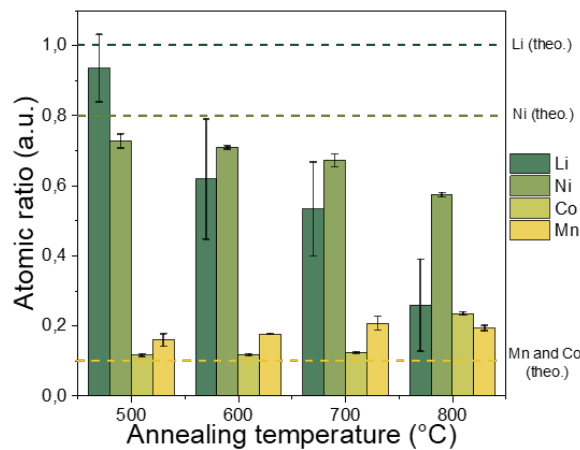


**Figure 12.** Atomic ratios estimating the surface stoichiometry of NMC thin films. The error bar was estimated as the semi-difference between the largest and smallest results within each set of measurements per sample.

As seen upon increasing temperature, the Li and Ni concentrations decrease in favor of slightly larger Co and Mn ones. It suggests densification of the surface towards a rock salt-like surface layer, which correlates well with the evolution of the Ni 2p spectra.

### 1.7.5 X-ray diffraction

The results of XRD characterizations reveal the unexpected formation of a  $\text{Li}_2\text{PtO}_3$  layered oxide for the Pt/NMC811 sample annealed at 800°C (Figure 13), that could corroborate the presence of Pt on the surface, as highlighted by the previous XPS analysis (Figure 9). The formation of this phase has never been reported in the case of annealed Pt/LiCoO<sub>2</sub> samples in numerous publications about R-3m LiCoO<sub>2</sub> or spinel oxide thin films and their use in all-solid-batteries. It may be explained by the higher basicity of the Ni-rich layered materials compared to LiCoO<sub>2</sub> (LiNiO<sub>2</sub> pH~13, LiCoO<sub>2</sub> pH~7) [16, 17]. Due to this reactivity of the NMC811 film with the platinum substrate and its possible consequences on the structure/composition of the electrode, alternative materials for the substrate/current collector had to be used, as discussed later.

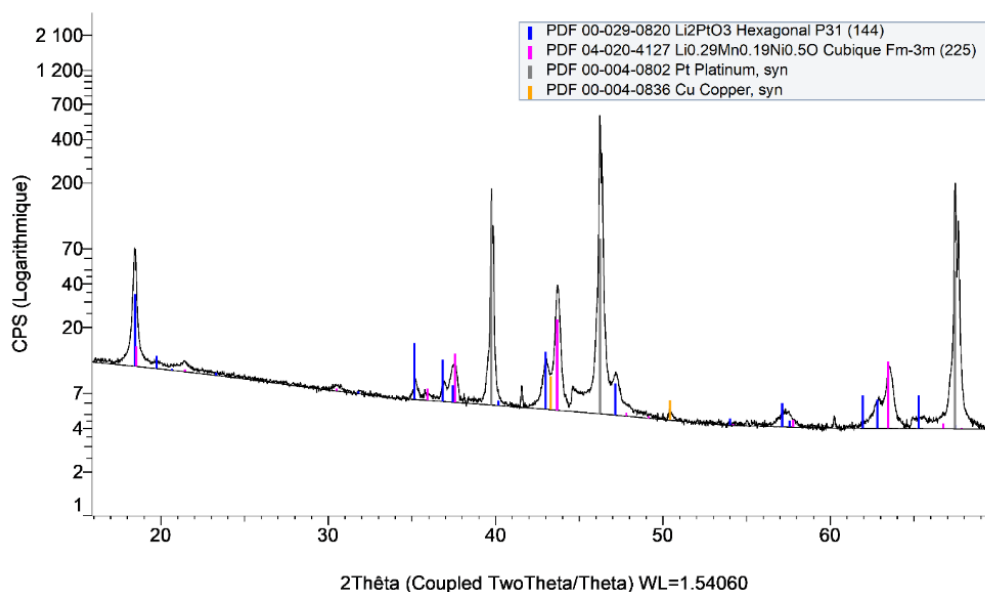


**Figure 13.** XRD pattern of NMC811 thin film sample annealed at 800°C.



### 1.7.6 Scanning electron microscopy

Figure 14 illustrates the morphology obtained by SEM of thin films annealed at 600°C and 700°C. Both samples present cracks that arise from the difference in terms of the coefficient of thermal expansion (CTE) between the NMC811 film and the platinum foil. As a consequence of the significant difference in thickness between the NMC film and the platinum foil, the substrate imposes its strain on the NMC film during the annealing cycle. Therefore, due to higher CTE of Pt ( $\sim 9.10^{-6} \text{ K}^{-1}$ ) compared to that of NMC811 ( $\sim 13.10^{-6} \text{ K}^{-1}$ ), thin films will obviously crack. The sample annealed at 600°C displays grains in the 40-300 nm range with an elongated shape, while the one treated at 700°C has smaller round-shape grains (20-40 nm). In addition, the sample annealed at a lower temperature exhibits fewer cracks. This result is quite unexpected since the increase in annealing temperature should lead to bigger grains and likely a higher amount of cracks. Further analysis needs to be carried out to understand the origin of this result.

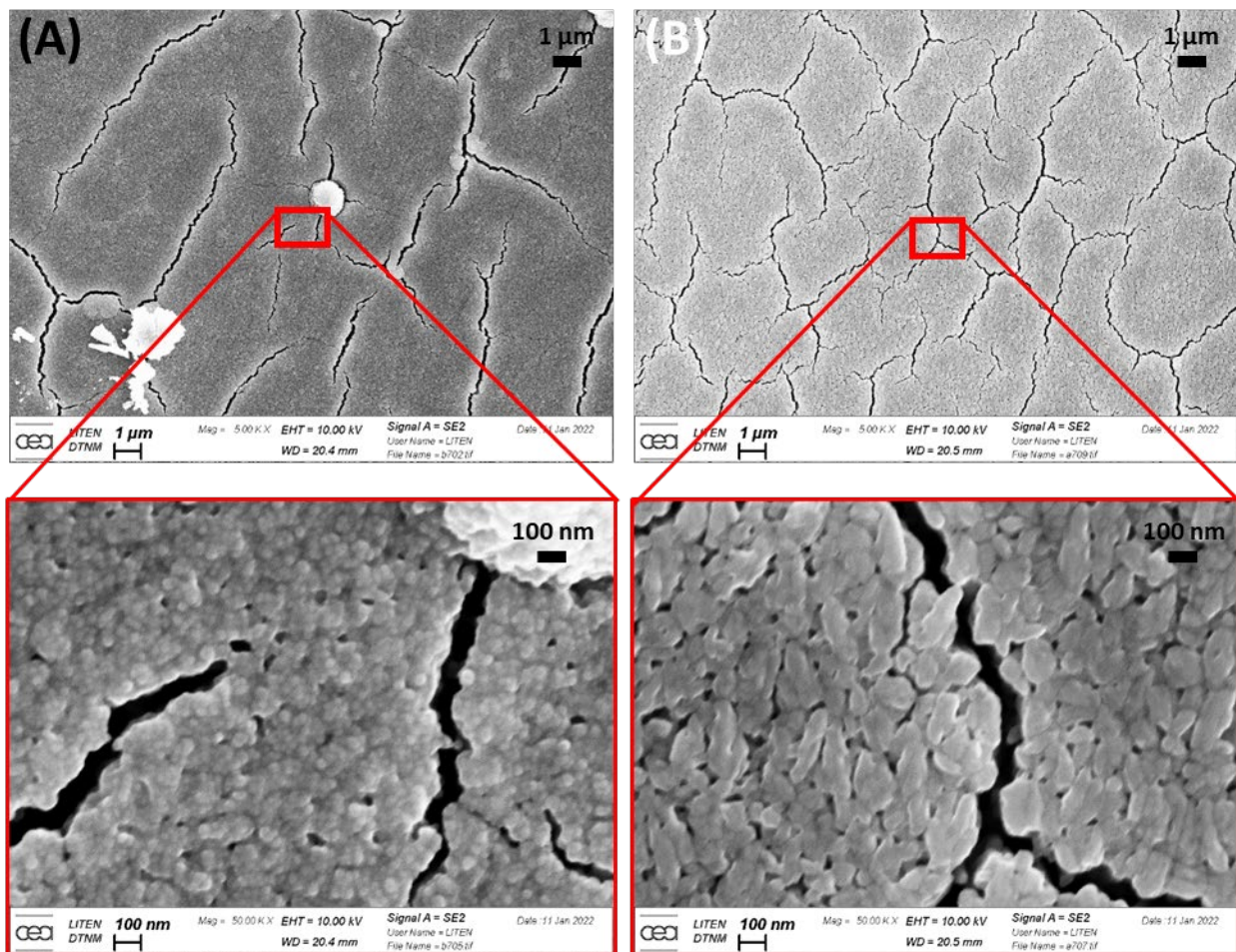


**Figure 14.** Influence of crystallization temperature on thin film morphology. SEM images of samples at different magnifications annealed at (A) 600°C (sample n° A7) and (B) 700°C (sample n° B2).

### 1.7.7 Conclusions

In conclusion, the combined Raman, XPS, XRD, and SEM analyses show a clear effect of the annealing temperature on the local structure of oxygen atoms in the NMC. This was associated with a change in the formal oxidation state of Ni and Co atoms upon annealing and the size of crystallites, as



reported in the SEM images. However, we also observed a reaction of the NMC811 thin films with platinum discs. Consequently, new investigations were carried out with gold discs.

## 1.8 Characterization of crystallized NMC811 thin films deposited on gold discs

Due to the reactivity of platinum discs with NMC811 thin films, new depositions were performed on 50  $\mu\text{m}$  thick and 12 mm large gold discs and annealed at temperatures from 500°C to 800°C from 5 min to 1 h by introducing/removing the sample at the given annealing temperature. Annealing was performed in the air due to technical constraints.

### 1.8.1 Electrochemical characterization

The same protocol as the one described previously was used for the fabrication of the cell. To avoid using an old LP57 electrolyte, we decided to use an equivalent electrolyte from another provider. Electrochemical analyses were performed at 25°C following the same procedure for all cells using a VMP3 Biologic apparatus:

1. Open circuit voltage for 5 min.
2. Five cycles at C/20 (charge and discharge) using a 200 mAh/g capacity between 3.0 V and 4.3 V Vs Li/Li<sup>+</sup>. The current density is about 2.5-2.9  $\mu\text{A}/\text{cm}^2$ .
3. Open the circuit voltage for 5 minutes after each charge and discharge.

Figure 15 displays the voltage profile of NMC811 thin. The voltage profiles are similar to the ones obtained from the crystallized NMC811 films on Pt discs. Indeed, the two successive plateaus, 4.0 V and 4.2 V Vs Li/Li<sup>+</sup> are still not visible. The highest capacities in the 140-150 mAh/g range are reached for short annealing at 700°C (20 min) or longer annealing (1 h) at 600°C. A straight comparison with results obtained with the previous NMC811 deposited on Pt discs cannot be done as annealing was performed in different conditions (in oxygen for 10 h). Nevertheless, similar values were obtained when annealing at a lower temperature of 500°C.

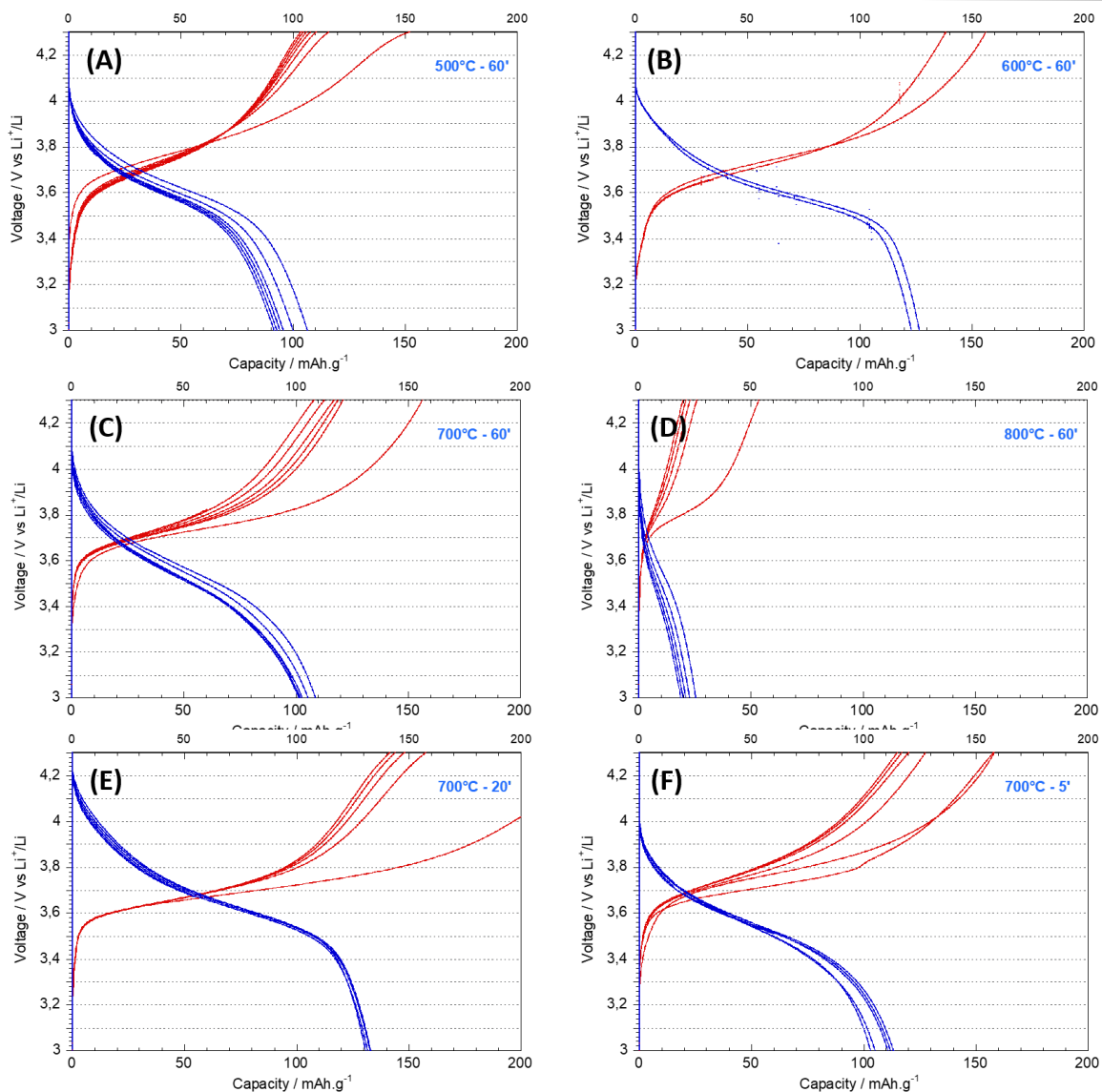


**Figure 15.** Influence of crystallization temperature on the galvanostatic charge/discharge of NMC811 thin films deposited on Au discs. Voltage versus Capacity of samples annealed at (A) 500°C, (B) 600°C, (C) 700°C and (D) 800°C for 1 h and annealed for (E) 20 min and (F) 5 min at 700°C. Five cycles were carried out at C/20 (charge and discharge) using a capacity of 200 mAh/g between 3.0 V and 4.3 V Vs Li/Li<sup>+</sup>.

### 1.8.2 Correlative analysis

Globally, similar results are observed for NMC811 thin films crystallized on Au discs compared to Pt discs, as depicted in Figure 16. Indeed, thin films still present cracks after annealing, and the EDS transition metal ratios are also in agreement with expected values (Figure 16(A, B)). In addition, as previously with Pt discs, upon increasing temperature, the Li and Ni concentrations decrease in favor of slightly larger Co and Mn ones (Figure 16(C)). For longer annealing duration at 700°C, there is not a clear trend, suggesting a possible crystallization already in 5 min (Figure 16(D)). Finally, the four thin film samples exhibit the characteristic response of NMC811 materials in a layered structure according to the Raman results [3]. Annealing temperature clearly modifies the relative intensities of the various bands, especially at 550 cm<sup>-1</sup>, thus revealing a modification of the cation coordination and/or oxidation state.

It is worth mentioning that no Au phase was detected on the film surface crystallized compared to Pt discs. This demonstrates not only the absence of a chemical reaction between NMC811 and Au disc but also the possibility of using gold as a substrate for further investigations.

Consequently, the development shown after the new combinatorial sputtering tool was carried out with Au discs.

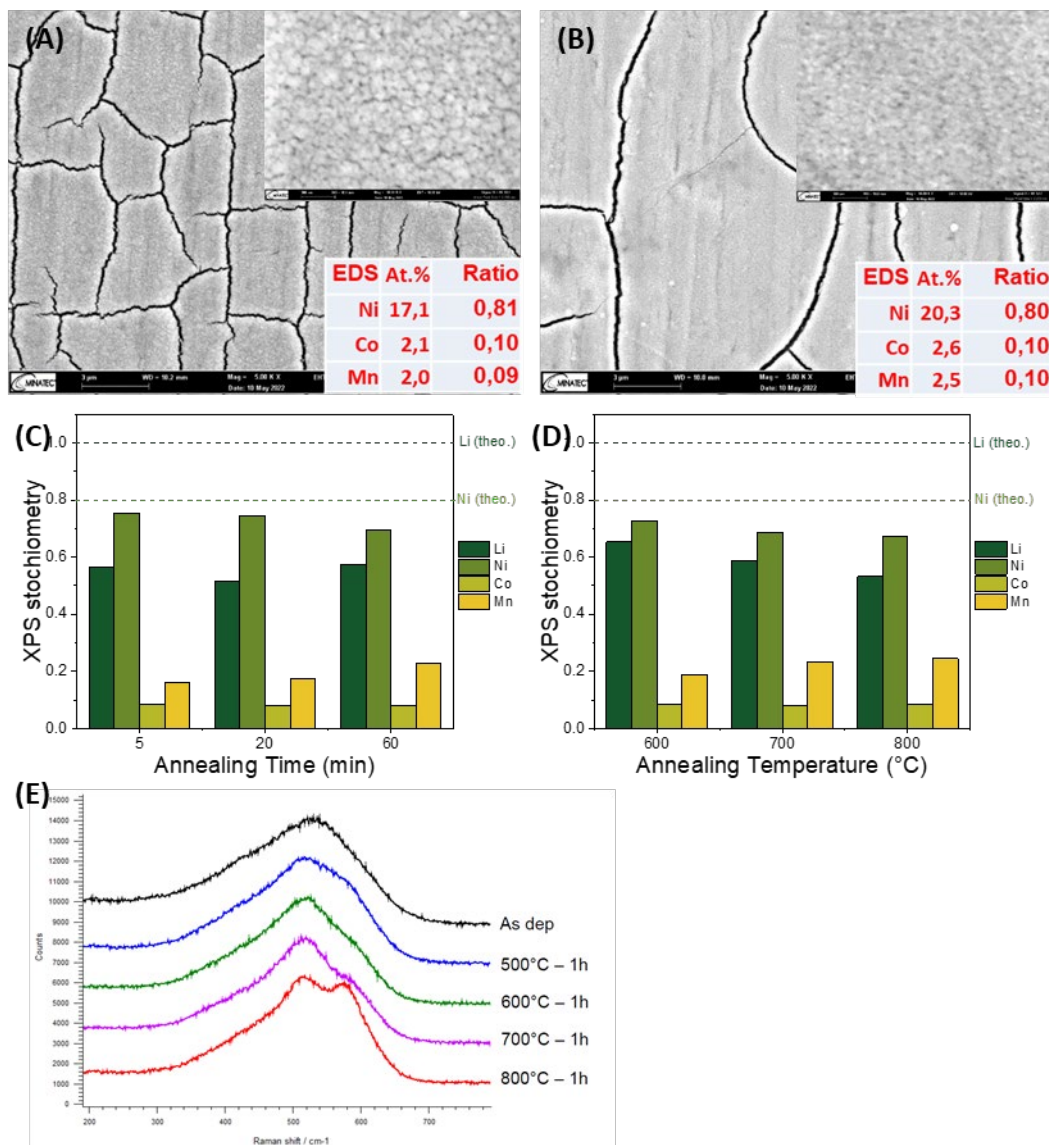


**Figure 16.** Correlative analysis of NMC811 thin films deposited on Au discs and crystallized in different conditions. (A) and (B) SEM images associated atomic ratios measured by EDS of samples annealed at 600°C and 700°C for 1 h. Influence of annealing conditions, (C) different durations at 700°C and (D) different temperatures for 1 h, on films stoichiometry measured by XPS. (E) Raman spectra for different temperatures for 1h.



## 2. Synthesis using the combinatorial magnetron sputtering tool and comparison (CEA/BASF)

### 2.1 Magnetron sputtering apparatus

As explained in the introduction, due to the fabrication delay of the combinatorial sputtering apparatus (mainly because of the Covid-19 situation), the combinatorial sputtering apparatus was installed at CEA only by the end of January 2022. Based on the experience developed with the alternative tool, CEA directly investigated the influence of the chamber pressure while setting the distance between the target and the substrate, the target power and the oxygen/argon flows. Here are the parameters:

- **Chamber pressure:** from 0.5 Pa to 4 Pa
- **Target power:** 3.8 W.cm<sup>-2</sup>
- **Target:** NMC811 and LNO from [Neyco](#)
- **Distance between the target and the substrate:** 8 cm
- **Oxygen:argon flow ratio:** 1:10
- **Deposition duration:** 3 h (for ICP-OES characterizations) and 6h (for physical-chemical and electrochemical characterizations)

As previously shown, two different substrates were used depending on the type of characterization techniques:

- **Glass substrates:** Two glass substrates, 76 x 26 mm, were fixed on the sample holder using Kapton tape on the upper part of the chamber: one for ICP-OES characterizations and one for mechanical profilometry measurement.
- **New gold discs, 14 mm in diameter and 100 μm thick,** were used to investigate the electrochemical response of the NMC thin film electrodes. Gold was chosen not only for its high thermal stability under oxygen or air but also to avoid its reactivity with NMC811 film, as demonstrated before. As shown in Figure 17, a new disc holder was specifically designed in the BIG-MAP frame to fix the gold discs properly. This disc holder allows for the maximization of the deposition on the disc (low shading) while properly maintaining the discs.

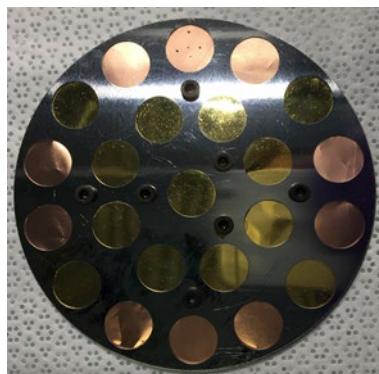
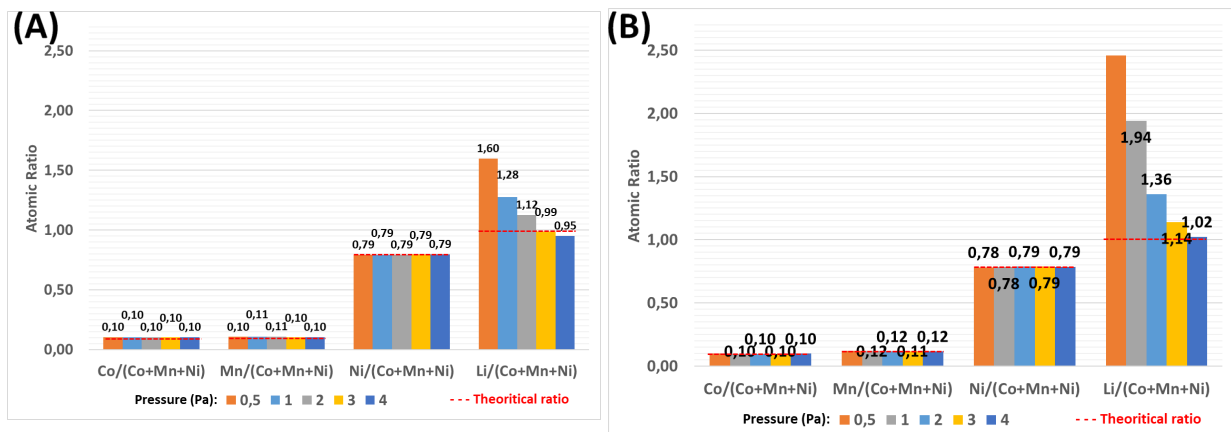


**Figure 17.** Image of the disc holder containing gold/copper discs. This disc holder is then fixed on the sample holder.



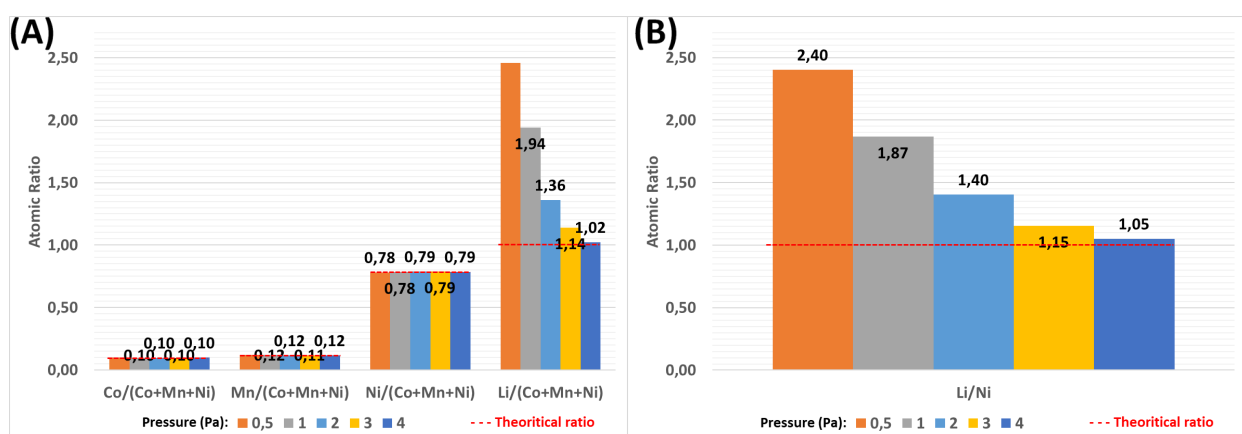
## 2.2 Comparison of chamber pressure influence between sputtering tools

Figure 18 depicts the evolution of NMC811 thin film atomic ratio as a function of the chamber pressure for (A) alternative and (B) combinatorial sputtering tool. The same trend was observed for both tools: no variations of the transition metal ratios and a decrease of the Li/transition metal ratio when pressure increases. It is worth mentioning that the new tool again obtained an operating point to reach stoichiometric NMC811 thin films. This pressure of 4 Pa is slightly higher than the alternative tool (3 Pa), which might come from the difference in chamber sizes.



**Figure 18.** Evolution of NMC811 thin film atomic ratio as a function of the chamber pressure for (A) alternative and (B) combinatorial sputtering tool. These atomic ratios come from ICP-OES characterizations.

In the meantime, we also investigated the evolution of the LNO thin film atomic ratio as a function of the chamber pressure using the combinatorial sputtering tool and a commercial LNO target (Neyco supplier). A similar trend and even Li/Ni ratios were obtained. Consequently, for LNO, an operating point to reach stoichiometric films is also reached at 4 Pa for LNO.



**Figure 19.** Evolution of (A) NMC811 and (B) LNO thin film atomic ratio as a function of the chamber pressure using the combinatorial sputtering tool (commercial target from Neyco). These atomic ratios come from ICP-OES characterizations.

To conclude, we were able to identify, for both tools, an operating point to reach stoichiometric thin films of NMC811 and LNO by playing on the chamber pressure.

## 2.3 Thickness distribution of NMC811 and LNO thin films

For NMC811 and LNO thin films, the thickness distribution was investigated using automatic mechanical profilometry, as shown in Figure 20. One can notice that the higher the pressure, the thinner the film. Indeed, at higher pressure, scattering of species is more likely, which reduces the deposition rate of the films. In addition, we can observe that the deposition rate is higher for LNO than NMC811; the reason for that is still unclear.

At the operating point of 4 Pa, the deposition rate of NMC811 is about  $2.5 \pm 0.4 \text{ nm}\cdot\text{min}^{-1}$  while a similar value of  $2.4 \text{ nm}\cdot\text{min}^{-1}$  was obtained for the alternative tool at the operating point (3.0 Pa). In the case of LNO thin films, the deposition rate is about  $3.6 \pm 0.6 \text{ nm}\cdot\text{min}^{-1}$ .

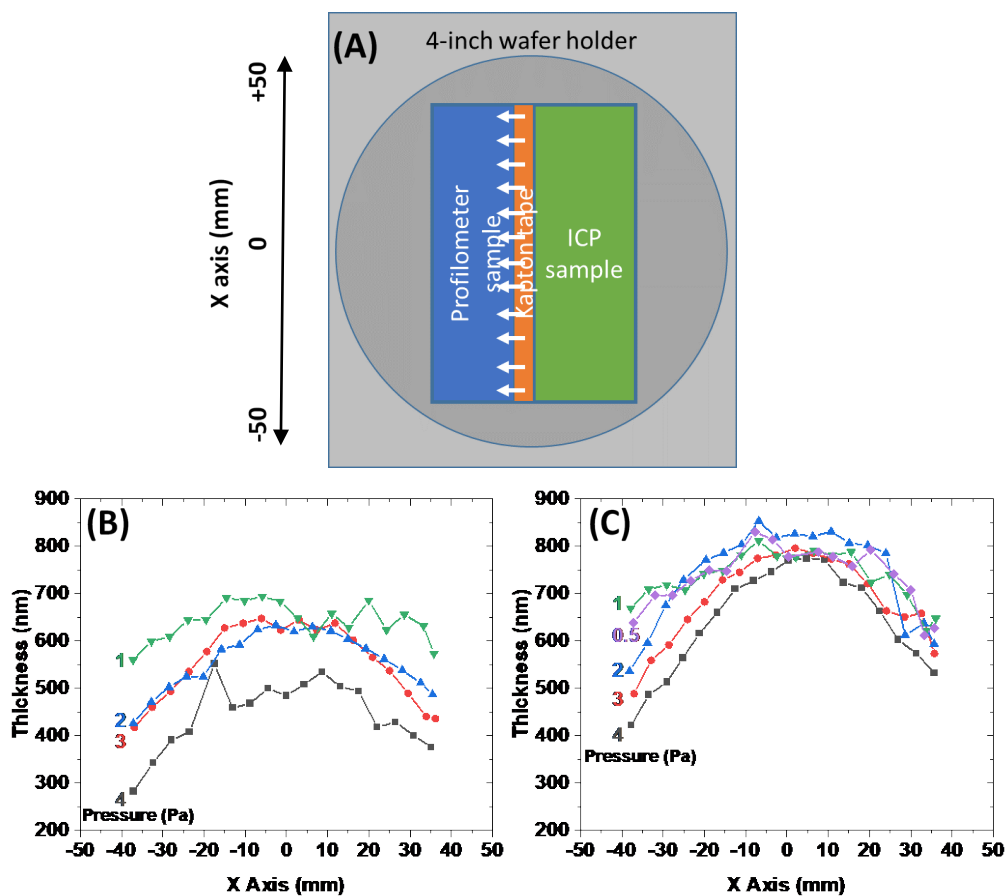


**Figure 20.** (A) Schematic representation of the substrate-holder carrying the sample for mechanical profilometry measurements. The white arrows indicate the measurement location. Evolution of (B) NMC811 and (C) LNO thin film thickness distribution. Deposition duration was fixed at 3 h.

## 2.4 Characterization of NMC811 thin films deposited on gold discs

### 2.4.1 Sample preparation

As previously, once the suitable stoichiometry was reached, we investigated the crystallization. The depositions were carried out on gold discs with a diameter of 14 mm. Prior to film deposition, the gold discs were cleaned in an HCl solution. Their individual weights were precisely determined using a microbalance (0.1  $\mu\text{g}$  resolution). The deposition was performed in the optimum conditions for 6 hours using the previous disc holder (Figure 17). After deposition, the samples were annealed in a tubular furnace for 1 h under oxygen flow at different temperatures (depicted in Table 3). The



furnace was heated to the given temperature in oxygen; once the temperature was reached, the samples were introduced. Finally, the samples were removed without cooling down the furnace and directly introduced in the glovebox to limit air exposition.

**Table 3.** Conditions of annealing for each sample.

Sample ID	Annealing T (°C)
B3, C5, H6	500
D3, F8, H8	600
B8, D8, F3	700
C6, H4, I3	800
E5	No annealing, reference

After deposition, samples were weighed again in a glovebox to determine the weight of the NMC811 thin film by subtracting the weight of the bare substrate. Figure 21 shows the NMC811 coating mass spread over the 4-inch wafer holder. The mass was measured after annealing for all samples except for E5, which was not annealed. The mass is  $0,440 \pm 110$  mg. Even though different annealing temperatures were used with possible  $\text{Li}_2\text{O}$  losses during annealing, this significant variation arises mainly from the limited homogeneous surface area in sputtering deposition, which is well-known. However, this will not be an issue as long as we know the coating mass for further electrochemical characterization.

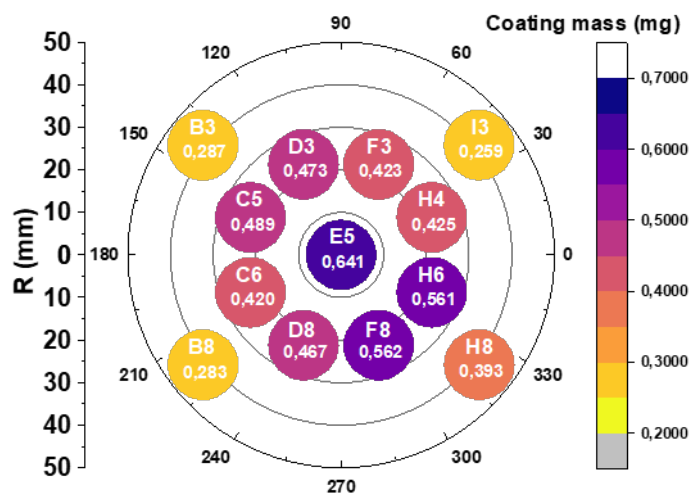


**Figure 21.** NMC811 coating mass spread over the 4-inch wafer-holder. The deposition duration was fixed at 6 h. The mass was measured after annealing for all samples except for E5, which was not annealed.

#### 2.4.2 Correlative analysis

The same workflow as shown before was realized in this new series of samples. Unfortunately, as shown in Figure 22, as-deposited and annealed samples present numerous contaminants, such as Al, Ti, W, Mo, Cl (which might come from the disc cleaning in the HCl solution), and Si. Consequently, the half-cells based on these crystallized NMC811 films displayed poor electrochemical response (not shown here).

	Ref		500		600		700		800	
	Position	%At Conc								
Mn 3p	48.95	2.16	49.08	2.6	49.1	3.88	49.41	4.89	48.95	4.14
Li 1s - NMC	53.67	8.91	53.72	5.07	53.9	0	54.27	1.9	53.93	0
Li 1s - org	54.98	10.88	54.67	2.92	54.91	3.46	55.19	10.76	54.97	2.32
Li 1s - LiF			55.75	2.65						
Li 1s - LiCl			56.42	7.71						
Au 4f					84	0.22				
Co 3p	60.24	0.92	60.3	0.83	60.17	1.5	60.68	1.46	60.19	2.23
Ni 3p	66.93	6.96	66.83	8.21	67.13	16.89	67.07	14.38	67.14	14.42
Si 2p					102.5	3.45	102.13	1.42	102.5	4.26
Cl 2p			198.75	13.86			198.75	0.18		
Cl 2s			269.63	15.78						
Mo 3d					232.38	0.6	232.75	0.19	233	0.39
W 4d					247.88	0.95			247.25	1.14
C 1s C-C	284.66	1.8	284.49	3.33	284.72	2.76	285.04	9.05	284.99	2.8
C 1s - C-O	285.88	1.87	285.88	2.1	285.56	3.17	286.51	1.04	285.51	4.09
C 1s - C=O	288.6	0.82	288.2	0.88	288.4	0.23	288.87	0.64	288.9	0.33
C 1s - CO32-	289.41	7.41	289.52	0.57						
O 1s - NMC	528.69	11.16	528.92	14.37	529.62	25.59	529.56	28.48	529.62	22.24
Defective NMC	529.76	5.01	529.72	5.73						
O 1s - WO3					530.6	3.64			530.48	2.93
O 1s - CO32-/C=O/MoO4/Ni-OH	531.15	30.91	531.25	3.23	531.4	10.94	531.4	9.05	531.31	19.77
O 1s - C-O/Si-O	532.53	3.96	532.81	0.95	532.59	5.53	532.69	2.09	532.55	4.44
Ni 2p	854.12	6.43	854.25	9.21	854.25	17.19	854.37	14.48	854.12	14.48

Figure 22. Influence of annealing temperature on thin film surface chemistry measured by XPS.

To identify the source of the contamination, CEA performed ICP-OES analyses (Figure 23) of the NMC811 target, LNO target, and NMC811 thin films (as-deposited) and compared the intensity levels of all elements with the blank. It evidences a clear contamination of aluminum, molybdenum, and tungsten within the commercial targets.

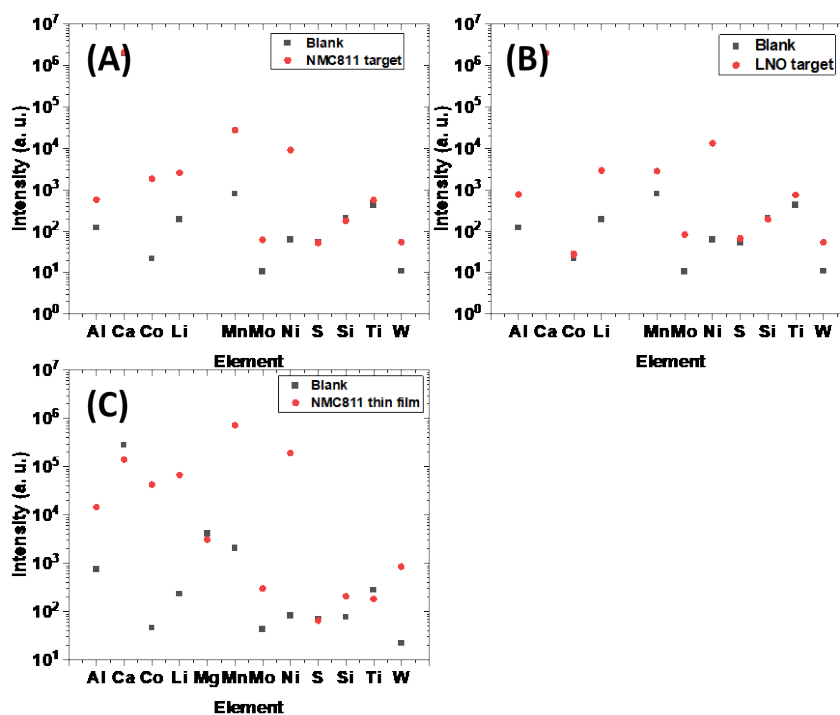


Figure 23. Identification of the contamination source by ICP-OES. ICP-OES intensity from A) NMC811 commercial target (Neyco supplier), B) LNO target (Neyco supplier), and C) NMC811 thin films (as-deposited) compared to the blank of different elements.



We believe that the crystallization issues are related to these contaminations from the commercial targets. Consequently, we decided to fabricate small targets using BASF powders.

## 2.5 Depositions and characterizations of LNO thin films, using targets from powder delivered by BASF, on gold discs

CEA produced small targets from LNO powders provided by BASF. The powders were cold-pressed and then annealed in an oxygen atmosphere. Right after the sintering, the target was introduced in the glovebox and glued onto a copper backing plate to be mounted on the sputtering cathode. As depicted in Figure 24, despite some irregularities on the target edges (on the right of the picture), the target was sintered correctly and ready to be used in the sputtering tool.

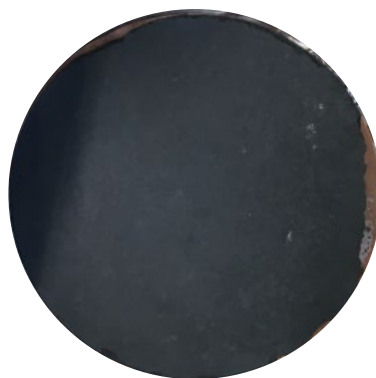


Figure 24. LNO targets fabricated from BASF powders.

Figure 25(A) depicts the thickness repartition of LNO thin films deposited from a commercial target and a homemade target using powder from BASF. As expected, the thickness variation is more pronounced for the homemade LNO target due to its smaller size. This dispersion is not an issue as long as the mass of the films is known for the electrochemical characterization. Figure 25(B) shows the microstructure of LNO thin films deposited on silicon wafers. The films appear dense with 50-100 nm large grains.

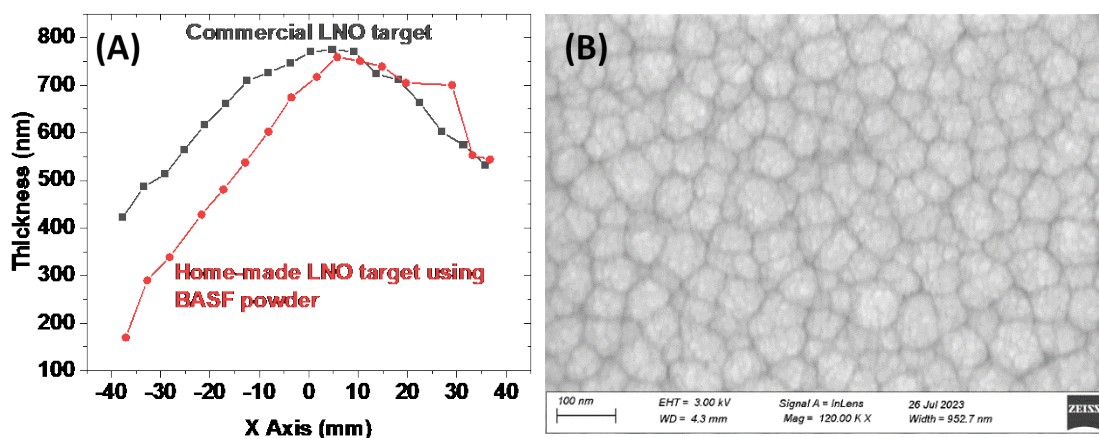
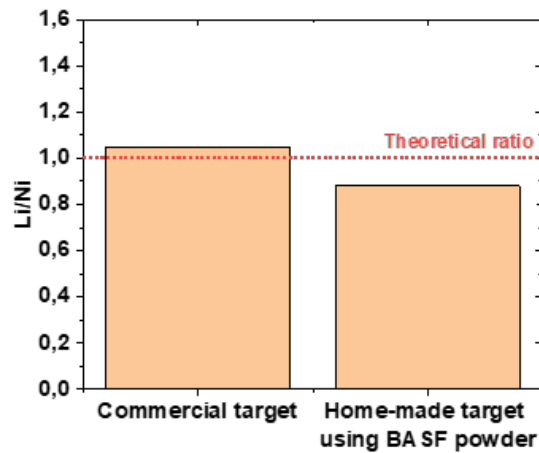


Figure 25. (A) Thickness repartition of LNO thin films deposited from a commercial and homemade target using BASF powder. (B) SEM image of LNO thin films deposited on a silicon wafer.



The Li/Ni stoichiometry was analysed by ICP-OES (Figure 26). The value obtained from the homemade target is lower (12%) than expected for the sputtering operating point. This discrepancy might come from a difference in stoichiometry between targets. As demonstrated before, reducing the chamber pressure will allow the value to be adjusted.



**Figure 26.** Comparison of Li/Ni atomic ratio, measured by ICP-OES, for LNO thin films deposited from a commercial target and from a homemade target using BASF powder.

Despite the slight sub-stoichiometry in Li, CEA performed crystallization of the thin films at different temperatures from 500°C to 800°C under an oxygen atmosphere. All the gold discs were weighed again after annealing, as seen in Figure 27(A). Then, these discs were assembled in half cells and cycled at C/20 ( $C=200 \text{ mAh.g}^{-1}$ ) between 3.0 and 4.3 Vs Li/Li<sup>+</sup> in EC:EMC, LiPF<sub>6</sub> electrolyte. Crystallisation temperatures have a significant influence on the voltage profiles, as depicted in Figure 27(B). The highest capacity is reached for an annealing temperature of 600°C. Even though the first charge capacity is lower than reported works of about  $240 \text{ mAh.g}^{-1}$  using a composite electrode [7], it can reach as high as  $180 \text{ mAh.g}^{-1}$  in planar thin film electrode without any binders or electronic conductor, which is an excellent result. The irreversible capacity loss is about 12 %, and the subsequent cycles display a coulombic efficiency of 97-98.5 %. It also exhibits very low polarisation. It seems that there are transitions in-between  $\sim 4.0 \text{ V Vs Li/Li}^+$  and  $\sim 3.5\text{-}3.6 \text{ V Vs Li/Li}^+$ , but they are not as visible as experimentally observed with composite electrodes [7]. Apart from different possible crystallization phases, the absence of the transitions can also arise from internal strains induced by the substrate, well-known for thin films.

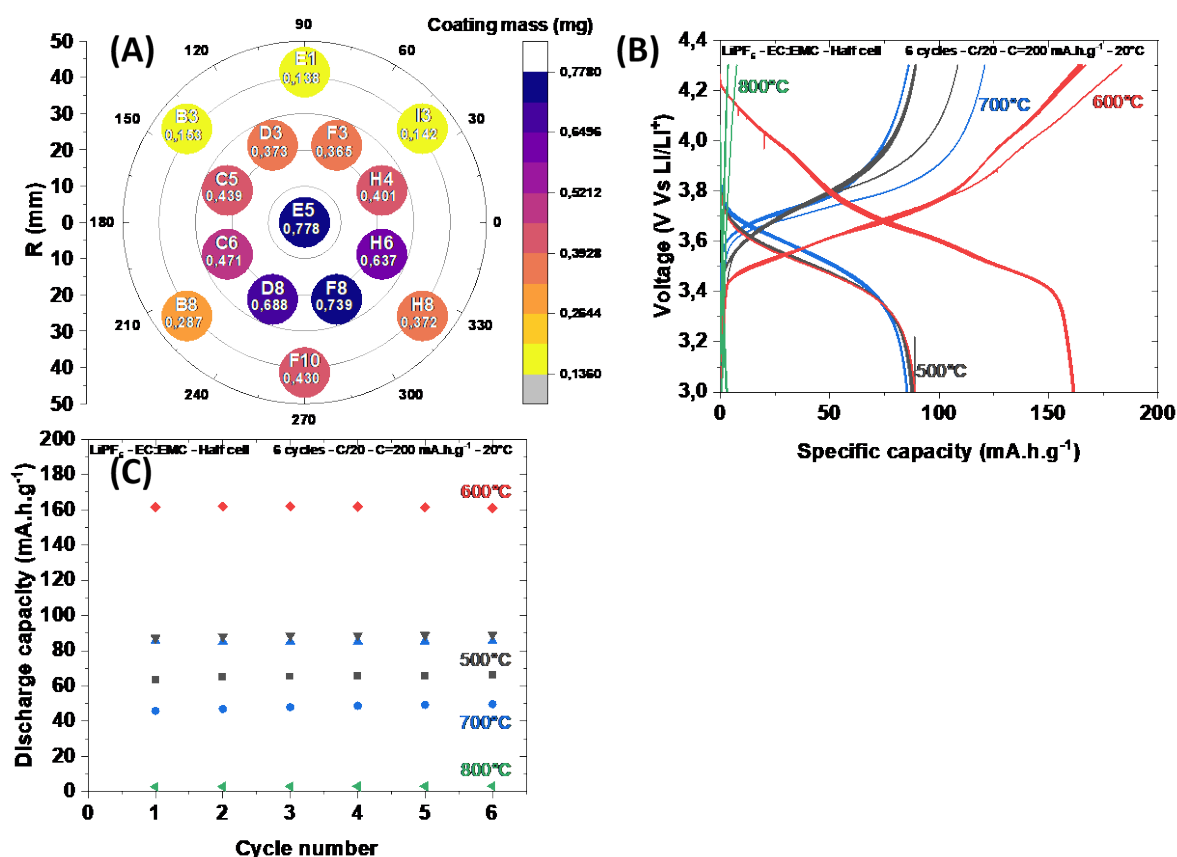


**Figure 27.** The influence of film crystallization temperature on electrochemical response. (A) Mass repartition, after crystallization, of LNO thin films deposited with a homemade target on 14-mm gold discs. (B) Six voltage profiles for each cell and (C) discharge capacity versus cycles of half-cells using LNO positive electrodes annealed at different temperatures.

XPS analysis was performed on the annealed LNO thin films (not shown here). As for the NMC811 ones shown previously (Figure 11), the LNO thin films show a mixed Ni<sup>2+</sup>/Ni<sup>3+</sup> oxidation state, which is hard to estimate. It seems that a larger amount of Ni<sup>3+</sup> is present for the ones annealed at 600°C. Other structural analysis characterization is in progress to understand further the optimum annealing temperature found for LNO.

### 3. High-throughput screening of thin film ionic conductor and liquid electrolyte (CEA/FZJ)

As explained in the introduction, the synthesis of combinatorial ionic conductor thin films carried out in task 4.5 has de facto to be combined with high throughput experimentation (HTE) characterization, performed in task 6.5. Due to the strong correlation between task 4.5 and task 6.5, the synthesis and the high throughput characterizations carried out by CEA were detailed in the deliverable D6.5. This HTE approach allowed us to identify an optimum LiPON composition with the highest ionic conductivity.



Similarly, high-throughput experimentation activities on electrolyte levels conducted by FZJ and associated with post-cycling analysis performed by other partners, including CEA, were reported in D6.5. This HTE approach allowed us to identify optimum concentrations of DTDPh and DCKEA functional additives for considered tier chemistries defined in the project.

## 4. Conclusions about the deliverable

Task 4.5 aimed at developing model Ni-rich layered thin film electrodes and an ionic conductor library later used as artificial CEI for these model electrodes, both synthesized by sputtering. As explained in the introduction, this deliverable focuses on the development of model electrodes using the procedure described in Figure 28 while, due to the inextricable correlation between this task and high-throughput screening characterizations carried out in task 6.5, the thin film library development was presented in D6.5, already reported.

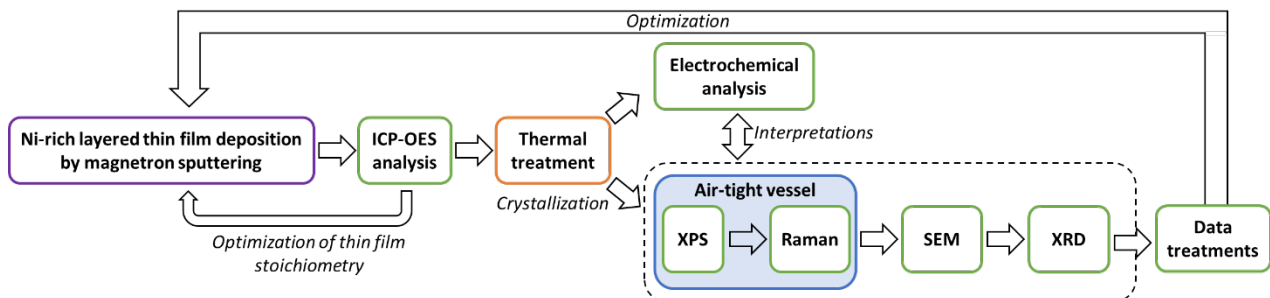


**Figure 28.** The methodology followed during CEA activity to realize and characterize the model Ni-rich layered thin film electrode deposited by sputtering.

Before going further, CEA first adopted a closed-loop methodology to adjust the stoichiometry of NMC811 and LNO thin films deposited by magnetron sputtering. To do so, the different sputtering parameters were varied, and their impact on the chemical compositions of the film by ICP-OES was investigated. An optimum sputtering operating point was found to obtain NMC811 and LNO thin films with chemical compositions close to the expected values.

After this crucial step, annealing treatments were investigated to crystallize the thin films deposited on platinum discs. Half-cells were then realized using these Pt/NMC811 samples to perform galvanostatic cycling, and, in the meantime, various physical-chemical characterizations (XPS, Raman, SEM, XRD) were carried out on other samples realized in the same conditions. These results suggest a reaction between the Ni-rich material and the platinum substrate during annealing. Consequently, the Pt substrates were replaced by Au discs, which allows proper annealing without any side reactions. Optimum annealing conditions were highlighted for both thin film electrodes, NMC811 and LNO, obtained from BASF. These thin film model electrodes exhibit a high first charge specific capacity of about 150 (NMC811) and 180 mAh/g (LNO), whereas no electronic conductor and binders are used.

In conclusion, through a workflow combining thin film deposition, annealing, electrochemical and physical-chemical characterization (XPS, Raman, XRD, and SEM-EDS), it is possible to follow with



different levels of interpretation (quick feedback to deep understanding), the chemical composition, qualitative and quantitative chemical structure in correlation to their electrochemical performances. Consequently, deposition conditions and crystallization step were optimized to develop stoichiometric and well-crystallized NMC811 and LNO thin film electrodes with interesting electrochemical responses. In the meantime, an ionic conductor library deposited by combinatorial sputtering and high-throughput characterization was also developed and thoroughly reported in D6.5.

This long development of thin film model electrodes and ionic conductor library coupled with high-throughput characterization was essential. Indeed, this thin film approach will then accelerate the identification of new artificial CEI for Ni-rich layered electrodes by stacking the model thin film electrode with the combinatorial thin film library. Up to 76 different protective layers will be simultaneously and electrochemically analyzed in contact with a given electrolyte (liquid or even solid) in order to quickly identify the best protective layer for a given electrolyte.

## 5. References

- [1] J. Fischer, C. Adelhelm, T. Bergfeldt, K. Chang, C. Ziebert, H. Leiste, M. Stüber, S. Ulrich, D. Music, B. Hallstedt, H. J. Seifert, "Development of thin film cathodes for lithium-ion batteries in the material system Li-Mn-O by r.f. magnetron sputtering", *Thin Solid Films* 528 (2013) 217 doi: 10.1016/j.tsf.2012.08.058
- [2] S. Cotte, B. Pecquenard, F. Le Cras, R. Grissa, H. Martinez, L. Bourgeois, "Lithium-rich manganese oxide spinel thin films as 3 V electrode for lithium batteries", *Electrochimica Acta* 180 (2015) 528, doi: 10.1016/j.electacta.2015.08.145
- [3] L. Baggetto, D. Mohanty, R. A. Meisner, C. A. Bridges, C. Daniel, D. L. Wood III, N. J. Dudney, G. M. Veith, "Degradation mechanisms of lithium-rich nickel manganese cobalt oxide cathode thin films", *RSC Adv.* 4 (2014) 23364, doi: 10.1039/c4ra03674c
- [4] M. Strafela, H. Leiste, K. Seemann, H. J. Seifert, S. Ulrich, "Influence of substrate surface roughness on microstructural and electrical properties of Lithium-rich Li-Ni-Mn-Co-O thin film cathodes", *Vacuum* 131 (2016) 240, doi: 10.1016/j.vacuum.2016.06.017
- [5] M. Jiang, X. Wu, Q. Zhang, D. L. Danilov, R.-A. Eichel, P. H. L. Notten, "Fabrication and interfacial characterization of Ni-rich thin-film cathodes for stable Li-ion batteries", *Electrochimica Acta* 298 (2021) 139316, doi: 10.1016/j.electacta.2021.139316
- [6] H.-K. Kim, T.-Y. Seong, Y.-S. Yoon, "Fabrication of a Thin Film Battery Using a Rapid-Thermal-Annealed LiNiO<sub>2</sub> Cathode", *Electrochem. Solid-State Lett.* 5 (2002) A252, doi: 10.1149/1.1510323
- [7] N. D. Phillip, R. E. Ruther, X. Sang, Y. Wang, R. R. Unocic, A. S. Westover, C. Daniel, G. M. Veith, "Synthesis of Ni-rich thin-film cathode as model system for lithium-ion batteries", *ACS Appl. Energy Mater.* 2 (2019) 1405, doi: 10.1021/acsaem.8b01982
- [8] B. Wang, J. B. Bates, F. X. Hart, B. C. Sales, R. A. Zuhr, J. D. Robertson, "Characterization of thin-film rechargeable lithium batteries with lithium cobalt oxide cathodes", *J. Electrochem. Soc.* 143 (1996) 3203, doi: 10.1149/1.1837188
- [9] C.-L. Liao, K.-Z. Fung, "Lithium cobalt oxide cathode film prepared by RF sputtering" *J. Power*



- Sources* 128 (2004) 263, doi: 10.1016/j.jpowsour.2003.09.065
- [1] H. J. Noh, S. Youn, C. S. Yoon, and Y. K. Sun, "Comparison of the structural and electrochemical properties of layered  $\text{Li}[\text{Ni}_x\text{Co}_y\text{Mn}_z]\text{O}_2$  ( $x = 1/3, 0.5, 0.6, 0.7, 0.8$  and  $0.85$ ) cathode material for lithium-ion batteries," *J. Power Sources*, vol. 233, pp. 121–130, Jul. 2013, doi: 10.1016/j.jpowsour.2013.01.063.
  - [2] K. Märker, P. J. Reeves, C. Xu, K. J. Griffith, and C. P. Grey, "Evolution of Structure and Lithium Dynamics in  $\text{LiNi}_{0.8}\text{Mn}_{0.1}\text{Co}_{0.1}\text{O}_2$  (NMC811) Cathodes during Electrochemical Cycling," *Chem. Mater.*, vol. 31, no. 7, pp. 2545–2554, Apr. 2019, doi: 10.1021/acs.chemmater.9b00140.
  - [3] C. Ghanty *et al.*, "Li<sup>+</sup>-Ion Extraction/Insertion of Ni-Rich  $\text{Li}_{1+x}(\text{Ni}_y\text{Co}_z\text{Mn}_z)\text{wO}_2$  ( $0.005 < x < 0.03$ ;  $y : z = 8 : 1$ ,  $w \approx 1$ ) Electrodes: In Situ XRD and Raman Spectroscopy Study," *ChemElectroChem*, vol. 2, no. 10, pp. 1479–1486, Oct. 2015, doi: 10.1002/celec.201500160.
  - [4] R. Azmi, M. Masoumi, H. Ehrenberg, V. Trouillet, and M. Bruns, "Surface analytical characterization of  $\text{LiNi}_{0.8-y}\text{Mn}_y\text{Co}_{0.2}\text{O}_2$  ( $0 \leq y \leq 0.4$ ) compounds for lithium-ion battery electrodes," *Surf. Interface Anal.*, vol. 50, no. 11, pp. 1132–1137, Nov. 2018, doi: 10.1002/sia.6415.
  - [5] A. Hariki, T. Uozumi, and J. Kuneš, "LDA+DMFT approach to core-level spectroscopy: Application to 3d transition metal compounds," *Phys. Rev. B*, vol. 96, no. 4, p. 045111, Jul. 2017, doi: 10.1103/PhysRevB.96.045111.
  - [6] N. Pauly, F. Yubero, F. J. García-García, and S. Tougaard, "Quantitative analysis of Ni 2p photoemission in NiO and Ni diluted in a  $\text{SiO}_2$  matrix," *Surf. Sci.*, vol. 644, pp. 46–52, Feb. 2016, doi: 10.1016/j.susc.2015.09.012.
  - [7] H. Li, N. Zhang, J. Li, and J. R. Dahn, "Updating the Structure and Electrochemistry of  $\text{Li}_x\text{NiO}_2$  for  $0 \leq x \leq 1$ ," *J. Electrochem. Soc.*, vol. 165, no. 13, pp. A2985–A2993, Sep. 2018, doi: 10.1149/2.0381813jes.